A Coarse-Grained Model for Polyglutamine Aggregation Modulated by Amphipathic Flanking Sequences

Kiersten M. Ruff,[1,2] Siddique J. Khan,[1] and Rohit V. Pappu[1,*]

[1]Department of Biomedical Engineering and Center for Biological Systems Engineering, and [2]Division of Biology and Biomedical Sciences, Computational and Systems Biology Program, Washington University in St. Louis, St. Louis, Missouri

SUPPORTING MATERIAL

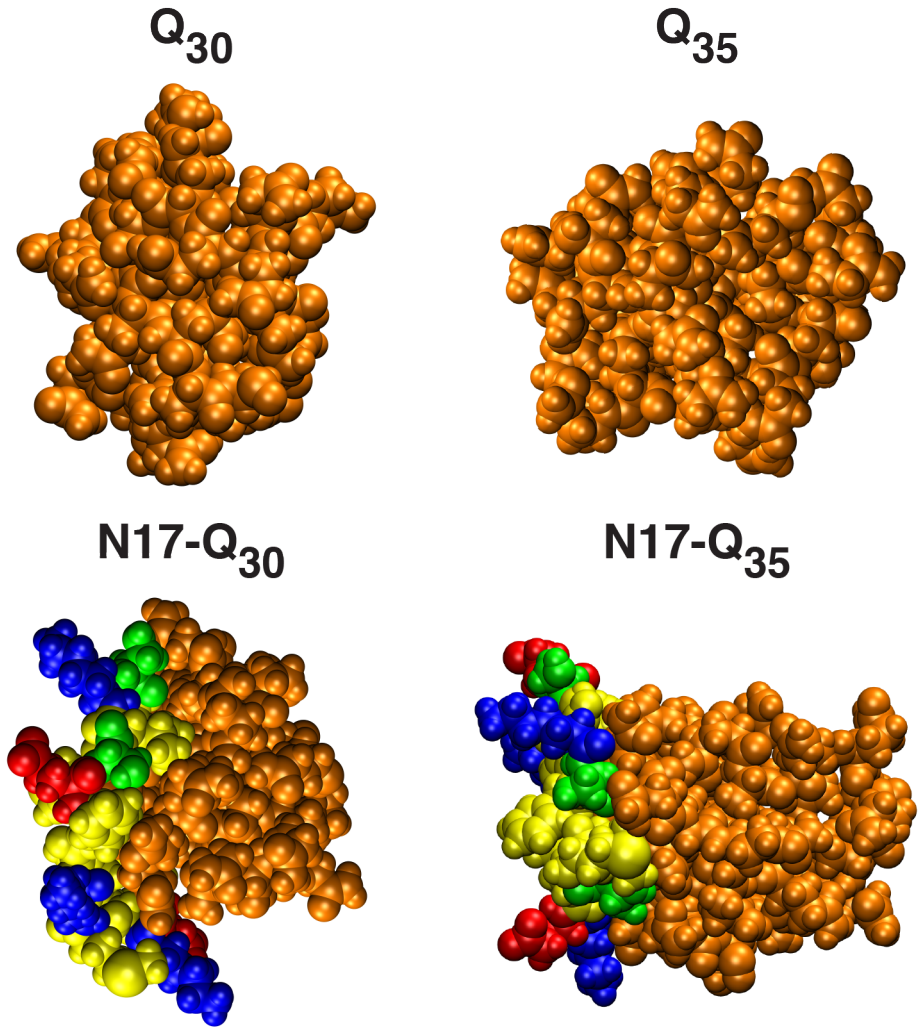

Fig. S1: Representative snapshots for Q_{30} and Q_{35} (top row) and N17-Q_{30}, N17-Q_{35} (bottom row) drawn from the simulated conformational ensembles of Williamson et al. (1). The color coding in the space filling models is as follows: orange spheres are for glutamine residues, yellow for hydrophobic, green for polar, blue for positively charged residues, and red for negatively charged residues. The drawings were made using the Visual Molecular Dynamics package (2).

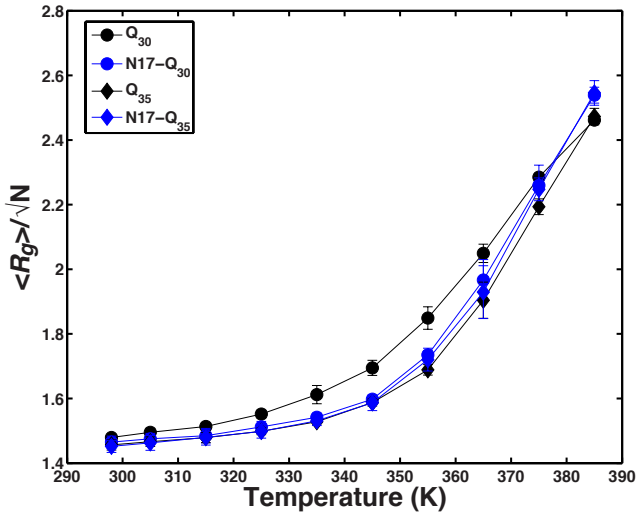

Fig. S2: Plot of the temperature dependence of the normalized average radii of gyration for Q_n and N17-Q_n (n=30, 35). In the temperature range of 298 K – 315 K, the normalized R_g values are similar for all four peptides implying that the densities of the corresponding globules are, on average, similar to each other.

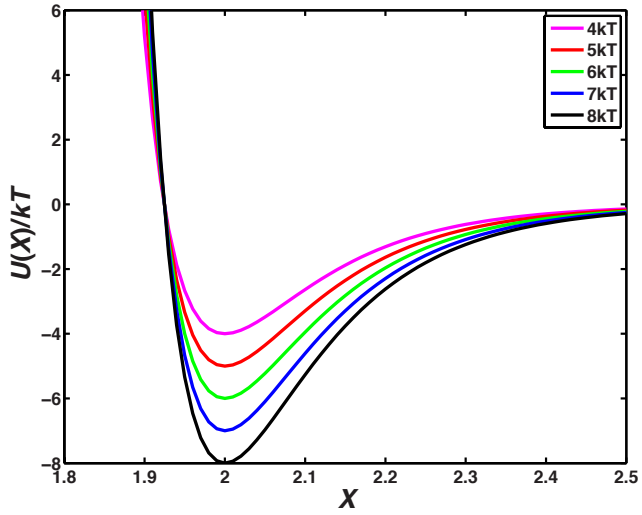

Fig. S3: Schematic of the calibration potentials. The figure plots the single well potentials based on Eq. (2) of the main text for different well depths. These were used in simulations of spherical particles to calibrate the overall energy scale that yields reliable aggregation and the steady state coexistence of small spherical aggregates with large, aspherical / linear aggregates.

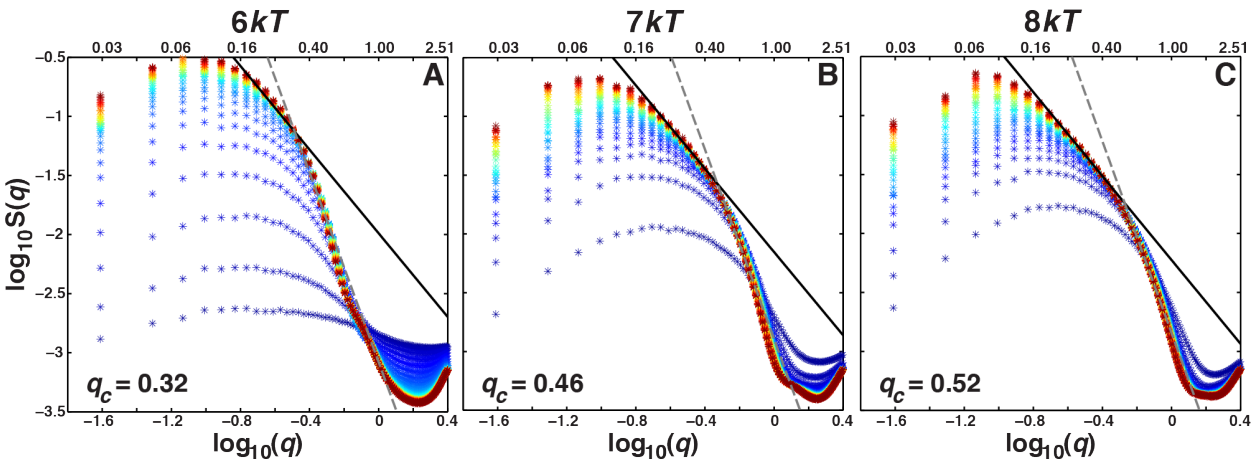

Fig. S4: Temporal evolution of the structure factors for the single well potentials shown in Fig. S3. These plots are shown for the three well depths that produce reliable small- and large-scale aggregation. As the well depth increases the crossover length scale q_c at steady state shifts to higher values. The values of q_c change minimally for well depths that are larger than $8kT$ and therefore, we choose an energy scale of $8kT$ in our simulations because this represents a sufficient level of supersaturation for a volume fraction of $f_v = 0.005$.

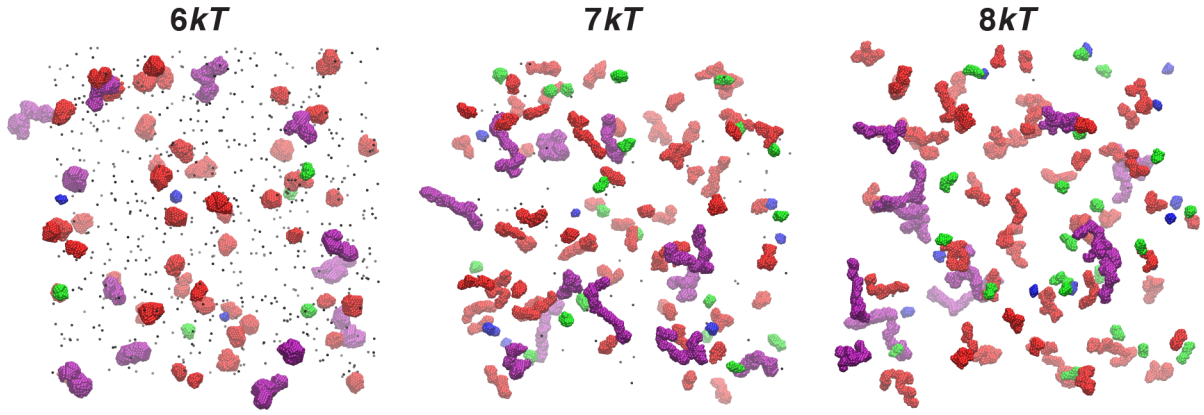

Fig. S5: Snapshots from the steady states for systems interacting via single well potentials with three different overall energy scales viz., $6kT$, $7kT$, and $8kT$, respectively. As the well depth increases, the steady state aggregate sizes become larger and show greater consistency with fibrillar morphologies. Molecules in the snapshots are colored according to the size of the corresponding aggregates *i.e.*, the number of molecules n within the aggregate to which they belong. The scheme is as follows: Black $\equiv n \leq 10$; Blue $\equiv 10 < n \leq 50$; Green $\equiv 50 < n \leq 100$; Red $\equiv 100 < n \leq 400$; Purple $\equiv n > 400$. The snapshots were generated using the Visual Molecular Dynamics package (2).

Section S1: Identifying the linear regimes in log-log plots of steady state structure factors
We identified the high-q and low-q regimes from log-log plots of the steady state structure factors with slopes of ca. –4 and ca. –1.8, respectively. These regions were determined using

sliding windows, each of length ten q-units. Additionally a restriction was added so as to not calculate the slope over very high q regions corresponding to length scales of only a few particles. Specifically, the minimum of the $S(q)$ versus q log-log plot was determined and a cutoff was defined such that the scanning windows ranged from the lowest q value (q=0.0245) to the q value that corresponded to minimum shifted by the cutoff (q_{cutoff}). Then the slopes were calculated over each of the sliding windows and the windows that corresponded to slopes with the minimum difference from –4 and –1.8 were selected for the high-q and low-q regimes, respectively. This procedure yields robust estimates for the slopes and regimes corresponding to the two slopes. It also enables reliable identification of the crossover length scales as evidenced by the low errors in our estimates of q_c.

Table 1: Linear regime details. The table shows the q intervals within which we identify the high- and low-q linear regimes. The values in the parentheses in the fourth and fifth columns denote the slopes found in each regime.

	q_{min}	q_{cutoff}	high-q regime	low-q regime
DPE-1	1.82	1.57	$1.18 \leq q \leq 1.40$ (–3.73)	$0.22 \leq q \leq 0.44$ (–1.81)
DPE-2	2.21	1.96	$1.08 \leq q \leq 1.30$ (–4.00)	$0.44 \leq q \leq 0.66$ (–1.82)
DNB	1.64	1.40	$0.96 \leq q \leq 1.18$ (–3.99)	$0.20 \leq q \leq 0.42$ (–1.82)
DWB	1.74	1.50	$0.98 \leq q \leq 1.20$ (–3.51)	$0.17 \leq q \leq 0.39$ (–1.82)

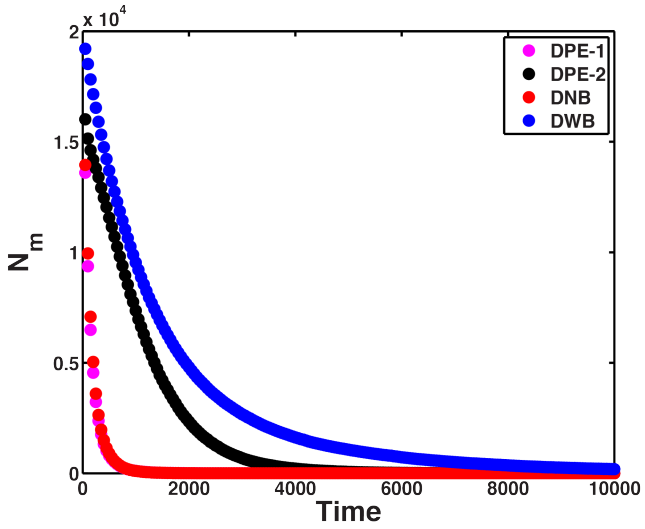

Fig. S6: Rates of loss of monomers into aggregates. These kinetic profiles are shown for the four models, DPE-1, DPE-2, DNB, and DWB. It is worth reiterating that loss of monomers into aggregates is a necessary albeit insufficient condition for achieving loss of fluorescence in the TMR assay. The additional requirement is for the formation of TMR dimers, which requires a high local concentration of TMR molecules and this is achieved in molecular aggregates with aggregation number that is generally larger than at least a 10-mer (3). Accordingly, the rates of monomer loss are less informative of the kinetics of aggregation of smaller species when compared to the development of structure in the high-q regime. Nevertheless, we see that the rates of monomer loss are faster for DPE-2 vis-à-vis DWB.

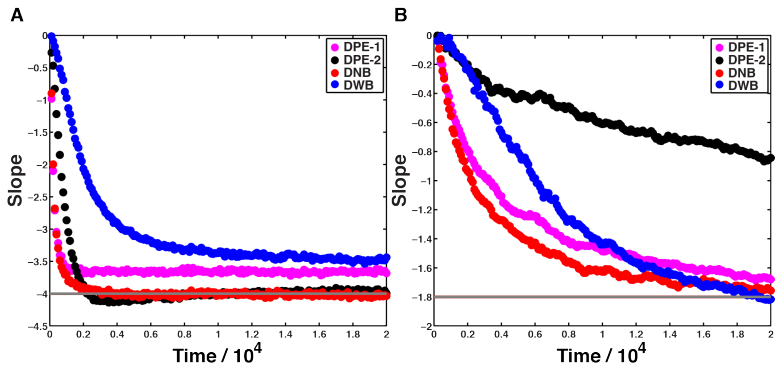

Fig. S7: Equivalent plot to Fig. 6 in the main text. This plot shows comparative assessments of the rate of change of slopes within the following high-q (left) and low-q regimes: $1.08 \leq q \leq 1.30$ and $0.17 \leq q \leq 0.39$, respectively. The former corresponds to the steady state high-q regime for the DPE-2 system and the latter corresponds to the steady state low-q regime for the DWB system.

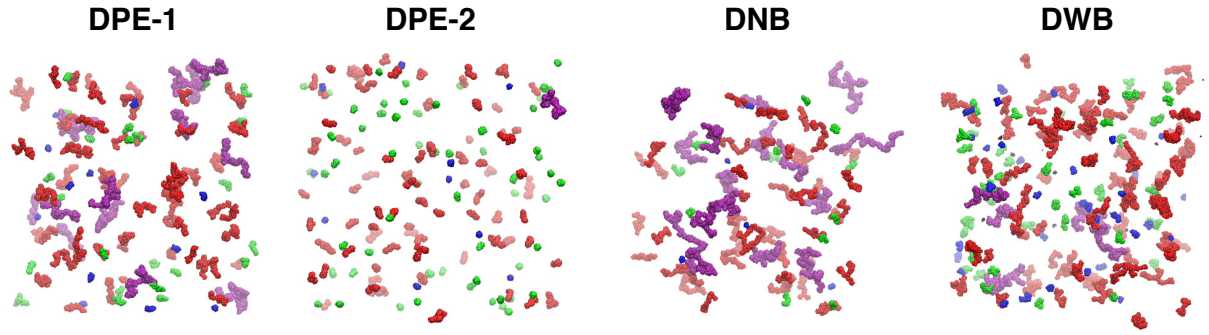

Fig. S8: Representative snapshots of the steady state aggregates that result from the simulations based on DPE-1, DPE-2, DNB, and DWB, respectively. Molecules in the snapshots are colored according to the size of the corresponding aggregates *i.e.*, the number of molecules n within the aggregate to which they belong. The scheme is as follows: Black $\equiv n \leq 10$; Blue $\equiv 10 < n \leq 50$; Green $\equiv 50 < n \leq 100$; Red $\equiv 100 < n \leq 400$; Purple $\equiv n > 400$. The snapshots were generated using the Visual Molecular Dynamics package (2).

References

1. Williamson, T. E., A. Vitalis, S. L. Crick, and R. V. Pappu. 2010. Modulation of Polyglutamine Conformations and Dimer Formation by the N-Terminus of Huntingtin. J. Mol. Biol. 396:1295-1309.
2. Humphrey, W., A. Dalke, and K. Schulten. 1996. VMD: visual molecular dynamics. J. Mol. Graphics Modell. 14:33-38.
3. Crick, S. L., K. M. Ruff, K. Garai, C. Frieden, and R. V. Pappu. 2013. Unmasking the roles of N- and C-terminal flanking sequences from exon 1 of huntingtin as modulators of polyglutamine aggregation. Proc. Natl. Acad. Sci. USA 110:20075-20080.